Journal of Hydrology 645 (2024) 132234

Contents lists available at ScienceDirect

Journal of Hydrology

journal homepage: www.elsevier.com/locate/jhydrol

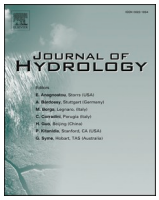

Research papers

Random fractional kinematic wave equations of overland flow: The HPM solutions and applications

Ninghu Su [a,b,*], Fengbao Zhang [a,c,*]

[a] State Key Laboratory of Soil Erosion and Dryland Farming on the Loess Plateau, Institute of Soil and Water Conservation, Northwest A&F University, Yangling, Shaanxi 712100, China
[b] College of Science and Engineering, James Cook University, Cairns, Queensland 4870, Australia
[c] Institute of Soil and Water Conservation, CAS and MWR, Yangling, Shaanxi 712100, China

ARTICLE INFO

This manuscript was handled by Corrado Corradini, Editor-in-Chief

Keywords:
Overland flow
Random fractional kinematic wave equation
Homotopy perturbation method (HPM) for solutions
Formulae for applications
Data from laboratory flow experiments
Parameter variability and interpretation

ABSTRACT

This paper presents new findings from analyses of a random fractional kinematic wave equation (rfKWE) for overland flow. The rfKWE is featured with orders of temporal and spatial fractional derivatives and with the roughness parameter, the effective rainfall intensity and infiltration rate as random variables. The new solutions are derived with the aid of a numerical method named the homotopy perturbation method (HPM) and approximate solutions are presented for different situations. The solutions are evaluated with data from overland flow flumes with simulated rainfall in the laboratory. The results suggest that on an infiltrating surface the temporal nonlocality of overland flow represented by the temporal order of fractional derivatives diminishes over time while the spatial nonlocality manifested by the spatial order of fractional derivatives continue if there is overland flow. It shows that the widely used unit discharge-height relationship is a special case of the solution of the rfKWE. Procedures are demonstrated for determining the fractional roughness coefficient, n_f, the order of spatial fractional derivatives, ρ, and the steady-state infiltration rate during the overland flow, A_s. The analyses of the data show that the mean spatial order of fractional derivatives is $\rho = 1.25$, the mean flow pattern parameter $m = 1.50$, and the mean fractional roughness coefficient is $n_f = 0.002$ which is smaller than the conventional roughness coefficient, $n = 0.108$. With these average values of the parameters and their standard deviations, simulations were performed to demonstrate the use of the methods, which is also a comparison of the classic KWE and rfKWE models.

1. Introduction

Overland flow is one of the major components in hydrological balance during rainfall, particularly during heavy rainfall for it is the source of runoff and floods, and it is also important during irrigation and snowmelt. It is a major cause of direct soil erosion which results in land degradation and many other indirect processes such as recharge to the subsurface flow, pollution of waterways and floods *etc*. Owing to its importance, this paper presents findings from theoretical analysis and experiments on overland flow to refine models and develop procedures for practical applications.

As it is known that overland flow can be described either by a full set of mathematical models in hydraulics, namely, the Saint-Venant equations, or their simplified forms such as the kinematic wave equation (KWE) (Lighthill and Whitham, 1955; Eagleson, 1970; Chow et al., 1988). For flow of small depths such as overland flow in many situations in the field conditions, the KWE model proposed by Lighthill and Whitham (1955) has been widely used and proven successfully after nearly seven decades of applications. In the KWE model, a simplified continuity equation is considered (Chow et al., 1988, p. 281) which makes the motion of overland flow as the consequence of the gravity force only due to the existence of the hydraulic friction gradient. Our earlier analysis using a fractional version of the KWE (fKWE) (Su and Zhang, 2022) indicated that the order of the space fractional derivatives is $\rho \sim 1.5$ rather than $\rho = 1$ in the KWE, which prompted the authors to investigate this model further.

To account for the growing evidence of space–time nonlocal properties in flow equations comparable to flow in porous media (Zhang et al., 2009), Harman et al. (2010), Kavvas and Ercan (2015, 2017) presented space–time fractional kinematic wave equations for open

* Corresponding authors.
E-mail addresses: ninghu.su@jcu.edu.au (N. Su), fbzhang@nwsuaf.edu.cn (F. Zhang).

https://doi.org/10.1016/j.jhydrol.2024.132234
Received 18 July 2024; Received in revised form 27 September 2024; Accepted 8 October 2024
Available online 26 October 2024

channel flow, which can be extended by considering the overland flow as a thin layer of channel flow. Zhang et al. (2016) proposed a distributed-order fractional dispersion-advection equation (dofADE) to model overland flow. The dofADE proposed by Zhang et al. (2016) captures the super-diffusive movement of water packets along preferential flow paths with the spatial fractional derivative and describes delays with the temporal fractional derivatives during the motion of water packets arising from soil heterogeneity and local topography on a slope.

This distributed-order time–space fractional partial differential equation (fPDE) for overland flow is very similar to the fPDEs for solute transport in soils (Zhang et al., 2009) so that the parameter's representations of the two types of physical processes can be investigated by analogue. As an extension of their dofADE, Zhang et al. (2017) examined the saturated subsurface flow on a hillslope, which starts with the Boussinesq equation (Eq. (3)) and simplified it using the well-known Dupui-Forchheimer assumption in groundwater hydrology resulting in a linear dofADE. The inclusion of a term with a distributed order in the fPDE for overland flow enables the model to explain the fast and slow components of flows on the hillslope in a way transport of solute is modelled in soils with large and small pores. With the dofADE, the slow movement of water and solute in soils and on hillslopes can be interpreted as a process of retention or jamming during transport by pores in soils and/or micro-topography on a hillslope. The dofADE by Zhang et al. (2017) can be regarded as a simplified form of the multi-term dofADEs presented by one of the present authors (Su, 2017). The fKWE was also proposed by one of the authors (Su, 2020) and Kavvas et al. (2021) for overland flow, and Kavvas et al. (2021) analysed it numerically with the finite difference method.

Many processes in nature are subject to random or stochastic variabilities, and overland flow and open channel flow are no exceptions. These random properties of overland flow are comparable to those of random flow in soils (Hopmans, 1989; Su, 2023). With these issues in mind for new formulae for practitioners in hydrology and environmental science, this paper presents a new version of the fKWE with random parameters for overland flow and develops new solutions for applications using the homotopy perturbation method (HPM).

2. The random kinematic and fractional kinematic wave equations

2.1. The kinematic wave equation of overland flow

For the cross sectional area of the flow, $A = wH$, with $H = H(x,t)$ being the depth of runoff and w the constant width, the conservation form of the continuity equation in the KWE due to Lighthill and Whitham (1955) takes the following form (Eagleson, 1970, p. 332; Chow et al., 1988, p. 275-289),

$$\frac{\partial H}{\partial t}+\frac{\partial q}{\partial x}=r(t)-i(t) \tag{1}$$

where q is the volumetric discharge of runoff per unit width (or unit discharge) $[L^2T^{-1}]$ or $q = Q/w$, where Q is the volumetric discharge $[L^3T^{-1}]$ and w the width of the flow; $r(t)$ is the effective rainfall intensity; $i(t)$ is the infiltration rate; x is the slope length, and t is time.

The momentum equation relating the unit volumetric discharge and the depth of runoff is more generally written as an empirical formula (Eagleson, 1970; Emmett, 1970),

$$q = cH^m \tag{2}$$

where m is a flow pattern parameter which varies for different types of flow: $m = 3$ for laminar overland flow, and $m = 5/3$ for fully turbulent overland flow (Eagleson, 1970, Eqs. (15) to (28); Emmett, 1970). The value determined experimentally for mixed flow in nature varies $5/3 \leq m \leq 3$ (Emmett, 1970), and the earlier observations from natural surfaces suggested that it is to be around $m \approx 2$ (Horton, 1938; Eagleson, 1970, p. 332). c in Eq. (2) is a parameter associated with the hydraulic gradient and the surface condition. For the flow velocity, the Manning equation is often used, which, with the SI units, is written as (Chow et al., 1988, Eq. (2.5.6)),

$$V=\frac{S_f^{1/2}R^{2/3}}{n} \tag{3}$$

where n is the Manning roughness coefficient with the dimension of $[TL^{-1/3}]$, S_f is the dimensionless friction slope, and R is the hydraulic radius.

On a planar surface, the wetted perimeter is simply the width of the cross section so that the hydraulic radius is $R = wH/w = H$. The KWE can be further simplified for flow with small depths where the friction slope for overland flow, S_f, is set to equal the slope gradient of the land surface, $S_0 = \tan\lambda_s$, where λ_s is the angle of the slope. With overland flow on a planar surface, the cross-sectional area of the flow is $A = wH$, and the unit discharge is $q = VH$. With the unit width and $R = H$, the Manning equation for the velocity and discharge is, respectively, written as

$$V=\frac{S_0^{1/2}}{n}H^{m-1} \tag{4}$$

and

$$q=\frac{S_f^{1/2}}{n}H^{m} \tag{5}$$

which implies that the parameter in Eq. (2) is $c=\frac{S_f^{1/2}}{n}$ and is approximated by $c=\frac{S_0^{1/2}}{n}$.

In the following sections, a fractional version of Eq. (1), and the related depth of flow, flow velocity, unit discharge and key parameters are investigated.

2.2. The random fractional kinematic wave models of overland flow

In recent years, an fPDE as another version of Eq. (1) known as the fKWE has been proposed (Su, 2020; Kavvas et al., 2021) and further analysed using laboratory data (Su and Zhang, 2022). In this paper, the fKWE is modified further on the following issues:

(1) random parameters are introduced to account for natural variations in the roughness of a hillslope, n_f, the rainfall intensity, $r(t)$, and infiltration rate, $i(t)$;
(2) a fractional order in time is introduced to account for the variability of the thin-film flow patterns on slopes which may resemble flow in porous media when irregular surfaces create fast and slow flow patterns.

Based on the earlier work of Su and Zhang (2022), a random fKWE or rfKWE to be analysed in this paper takes the form of

$$\tau^{\alpha-1}\frac{\partial^{\alpha}H}{\partial t^{\alpha}}+\frac{S_0^{1/2}}{n_f}\frac{\partial^{\rho}H^m}{\partial x^{\rho}}=r(t)-i(t) \tag{6}$$

where α and ρ are the orders of Caputo's fractional derivatives (Podlubny, 1999) which are more convenient for solving initial-value problems, and τ is a dimension correction factor (Kilbas *et al.*, 2006).

In the previous paper (Su and Zhang, 2022), it was shown that the fKWE is able to better explain the spatial nonlocality of overland flow, and that the order of fractional derivatives is around $\rho \approx 1.5$ for overland flow on indoor experimental flumes, and $\rho \approx 2.0$ for overland flow on longer slopes with data by Emmett (1970). This result enhanced our curiosity as to how a time–space fractional version of the model

performs in describing overland flow with random parameters.

The fractional approach interprets the *nonlocality* property of transport processes in the flow process. The *nonlocality* explains that the concentrations of a tracer, flow velocity or any other quantities at previous times and/or upstream locations contribute to the variation of the concentration or fluid velocity at the point of observation due to an uncertain velocity field. The *spatial nonlocality* means that the change in the concentration, flow velocity or any other quantities at the point of observation depends on its upstream value while the *temporal nonlocality* implies that the change in the concentration, flow velocity or any other quantities at the point of observation depends on the prior concentration, flow velocity or any other quantity loading (Benson et al. 2013). The spatio-temporal nonlocality implies scale-dependence and history-dependence which can also be described by non-linear integer PDEs (Su, 2020).

By introducing the random roughness coefficient, n_f, random rainfall intensity, $r(t)$, and random infiltration rate, $i(t)$, the analysis with the rfKWE will be compatible with models for random infiltration where parameters in an equation of cumulative infiltration or infiltration rate are random variables with certain distributions (Su, 2023). The inclusion of the random roughness coefficient also conforms to the patterns of natural surfaces which are more random or stochastic rather than deterministic (Kuipers, 1957; Burwell et al., 1963; Allmaras et al., 1966; Zobeck and Onstad, 1987; Su, 2023).

In the conventional KWE and in Eqs. (3) and (4) with the dimensionless friction slope S_f, the dimension of n is TL^{m-2}. In the fractional version in Eq. (6), either the new roughness parameter, n_f, embraces the newly introduced dimensions or another new parameter is added (Kilbas *et al.*, 2006, p. 464) so that the rest of the dimensions in Eq. (6) remain unchanged. Here no new parameter is introduced in Eq. (6) and with the dimensionless slope S_0, the dimension of n_f is $TL^{m-\rho-1}$, which, for $\rho = 1$, becomes TL^{m-2} which recovers the original dimensions in the KWE. As a widely accepted procedure, it is often convenient to use $S_0 = S_f$ so that the analysis can be simplified, which is also used in this paper.

3. Solutions of the fractional kinematic wave equation using the homotopy perturbation method with different forms of rainfall and infiltration rates

In this section, a widely used semi-analytical method, namely the homotopy perturbation method (HPM), which is also called a numerical method in the literature, is applied to derive solutions of the rfKWE, and the applications of the solutions are demonstrated as examples with data from laboratory experiments.

3.1. A brief overview of the homotopy perturbation method

The traditional numerical methods such as the finite difference, finite elements, and finite volume *etc*. are well known, and extensively used. In the 1970 s, an iterative method was developed by Adomian (1970, 1976, 1990) to solve differential equations, which is now widely known as the Adomian decomposition method (ADM). In the 1990 s, Liao (1992, 1995, 1997) developed a more generic method of this kind known as the homotopy analysis method (HAM) for nonlinear problems. In the late 1990 s, He (1999, 2003) simplified Liao's HAM to develop the homotopy perturbation method (HPM).

Chowdhury et al. (2009) demonstrated that the HAM is a generic method which can be reduced to both ADM and HPM. Sajid and Hayat (2008) also showed that the HPM is a special case of the HAM by setting $h = -1$ in Liao's (1992, 1997) HAM. These three methods have been extensively used to develop semi-analytical or numerical solutions for ordinary differential equations (ODEs), partial differential equations (PDEs), and their fractional counterparts such as fractional differential equations (fDEs) and fractional PDEs (fPDEs).

Compared to traditional numerical methods which require an initial condition (IC) and one or two boundary conditions (BCs) as essential requirements to derive solutions of the PDEs, ODEs and their fractional counterparts, the advantages of these decomposition methods are their abilities to solve these equations with only an IC (Yildirim and Kocak, 2009) or one BC or two-point BCs (He, 2003; Rajabi et al., 2007; Ates and Zegling, 2017). In such cases, the IC is not essential for a solution of these equations when the HPM or HAM is used. However, the IC and BCs are essential in many physical problems, and Laplace transform can be used to incorporate the IC, then the HPM or HAM is used to develop a solution of the problem (Javidi and Raji, 2011; Javidi and Ahmad, 2013). In this paper the rfKWE is transformed using the Laplace transform by incorporating the IC, then the transformed rfKWE is solved using the HPM for its solutions with the two-point BCs relevant to overland flow.

3.2. Solutions of the rfKWE for the depth, velocity and unit discharge of overland flow with the rainfall intensity and final infiltration rate as random variables

3.2.1. Depth of the overland flow

The essential background of the HPM is presented in Appendix B, and the key details of the series decomposition solution are presented in this section. The solutions of Eq. (6) are presented below subject to the following generic IC and BCs,

$$H(x,t) = f(x), \quad t = 0, x > 0 \tag{7}$$

$$H(x,t) = H_0, \quad t > 0, x = 0 \tag{8}$$

and

$$H(x,t) = H_L, \quad t > 0, x = L \tag{9}$$

These IC and BCs state that the initial water profile on the slope is $f(x)$, the depths of water on the upper and lower boundaries are, respectively, H_0 and H_L. These descriptions are generic and apply to situations when there is an initial depth of water on the slope, $f(x)$, before new runoff develops from the rainfall excess when the condition $r(t) - i(t) > 0$ is met. This situation is simplified for $f(x) = 0$ when there is no overland flow on the surface, which is the case to be considered here.

In addition to the IC and BCs, the following rate of infiltration, $i(t)$, based on the earlier works by Su (2014, 2020, Eq. (6.60)) is

$$i(t) = A_s + \left(\frac{\beta S}{2\lambda - 1}\right) t^{\lfloor \beta/(2\lambda-1) \rfloor - 1} \tag{10}$$

where A_s is the final infiltration rate on a hillslope, β is the order of time fractional derivatives, λ is the order of space fractional derivatives, t is time, and S is the sorptivity given by

$$S = \frac{(2\lambda - 1)(\theta_s - \theta_i)}{2\lambda} \left[\frac{D_0^2 \Gamma(1-\beta)\Gamma(2\lambda)}{K_0 \cos\lambda_s}\right]^{1/(2\lambda-1)} \tag{11}$$

with $\Gamma(1-\beta)$ and $\Gamma(2\lambda)$ being gamma functions, θ_s and θ_i the saturated and initial water ratios, K_0 the hydraulic conductivity, D_0 the diffusivity and $\cos\lambda_s = S_0$ the slope with the λ_s as the angle of the slope (Su, 2020) based on the works of Philip (1991) and Su (2014). A simpler equation of infiltration presented earlier (Su, 2010) can be used too. It should be noted that the stochastic description of infiltration in terms of integer calculus (Hopmans, 1989) and random models based on fractional calculus (Su, 2023) are compatible with the analysis of runoff processes using the random models.

The Laplace transform method can be applied to derive solutions of both deterministic and random differential equations and their fractional counterparts such as rfDEs and rfPDEs. The procedures used here are based on the random Laplace transform method demonstrated by Casabán et al. (2015) and mean square Laplace transform by Burgos et al. (2022; Villafuerte et al., 2010).

With $i(t)$ given by Eq. (10) and a random rainfall intensity, $r(t) = r_0$, denote $R_e = r_0 - i(t)$. Applying the random Laplace transform to Eq. (6), the IC and BCs in Eqs. (7), (8) and (9) yields,

$$\frac{S_0^{1/2}}{n_f}\frac{d^\rho}{dx^\rho}\left[\widetilde{H}^m(x,s)\right] + \tau^{\alpha-1}s^\alpha\widetilde{H}(x,s) = \widetilde{R}_e(s) - \sum_{k=0}^{n-1} s^{\rho-k-1}f^{(k)}(x) \tag{12}$$

where $f^{(k)}(x)$ is the integer-order differentiation of the initial condition, $f(x)$, with $n-1 \le \rho \le n$ (Podlubny, 1999, p. 106) and

$$\widetilde{R}_e(s) = \left(\frac{r_0 - A_s}{s}\right) - \frac{\beta S}{2\lambda - 1}\frac{\Gamma[\beta/(2\lambda-1)]}{s^{\beta/(2\lambda-1)}} \tag{13}$$

where $\Gamma[\beta/(2\lambda-1)]$ is the gamma function of $\beta/(2\lambda-1)$, and s is the Laplace transform variable. The BCs are now transformed to

$$\widetilde{H}(x,s) = \frac{\widetilde{H}_0}{s}, \quad x = 0 \tag{14}$$

and

$$\widetilde{H}(x,s) = \frac{\widetilde{H}_L}{s}, \quad x = L \tag{15}$$

In many situations such as experiments described in this paper, there is no initial overland flow on the slope surface so that $f(x) = 0$, and in such cases and with the following substitutions,

$$\widetilde{g}(x,s) = \widetilde{H}^m(x,s) \tag{16}$$

and

$$\eta = \frac{x}{L} \tag{17}$$

Eq. (12) is then written as follows,

$$\frac{S_0^{1/2}}{n_f}\frac{d^\rho\widetilde{g}(\eta)}{d\eta^\rho} = \widetilde{R}_e(s) - \tau^{\alpha-1}s^\alpha\widetilde{g}^{1/m}(\eta) \tag{18}$$

and the BCs become,

$$\widetilde{g}(\eta) = \widetilde{g}_0, \eta = 0 \tag{19}$$

and

$$\widetilde{g}(\eta) = \widetilde{g}_L, \eta = 1 \tag{20}$$

The solutions of Eq. (18) subject to the conditions in Eqs. (19) and (20) are outlined below using the HPM, which consists of an infinite series of steps with the first component of the solution as the basis to construct the next component of the solution. The background and the detailed derivation of the solution of Eq. (18) subject to the conditions in Eqs. (19) and (20) are given in Appendix B, and the solution is expressed as

$$\widetilde{g}(\eta) = \sum_{k=0}^{\infty} v_k(\eta) \tag{21}$$

and a two-term approximation is considered in this paper, namely, the approximate solution of Eq. (18) is given as

$$\widetilde{g}(\eta) = v_0 + v_1 \tag{22}$$

The procedures for the solution of Eq. (18) derived using the HPM are as follows (Ates and Zegling, 2017),

$$\begin{cases} \dfrac{S_0^{1/2}}{n_f}\dfrac{d^\rho\widetilde{g}(\eta)}{d\eta^\rho} + p\left[\tau^{\alpha-1}s^\alpha\widetilde{g}^{1/m}(\eta) - \widetilde{R}_e(s)\right] = 0 \\ \widetilde{g}(0) = \widetilde{g}_0,\ \widetilde{g}(L) = \widetilde{g}_L \end{cases} \tag{23}$$

where p is the perturbation parameter, and its range of variation is $0 \le p \le 1$. The first component is, for $p = 0$,

$$\begin{cases} p^0 : \dfrac{S_0^{1/2}}{n_f}\dfrac{d^\rho\widetilde{g}(\eta)}{d\eta^\rho} = 0 \\ v_0(0) = \widetilde{g}_0,\ v_0(L) = \widetilde{g}_L \end{cases} \tag{24}$$

which has the following solution after applying inverse Laplace transform, which is similar to the solution of an fDE given by Benchohra et al. (2009, Eq. (3) for $h(s) = 0$), and Ates and Zegling (2017, Eq. (15)),

$$v_0(\eta) = \widetilde{g}_0 + (\widetilde{g}_L - \widetilde{g}_0)\eta \tag{25}$$

The next order of the decomposed solution makes use of $v_0(\eta)$ from Eq. (25) in the fDE in Eq. (23) but with different BCs to yield (Ates and Zegling, 2017)

$$\begin{cases} p^1 : \dfrac{S_0^{1/2}}{n_f}\dfrac{d^\rho v_1(\eta)}{d\eta^\rho} + p\left[\tau^{\alpha-1}s^\alpha v_0^{1/m}(\eta) - \widetilde{R}_e(s)\right] = 0 \\ \widetilde{g}(0) = 0,\ \widetilde{g}(L) = 0 \end{cases} \tag{26}$$

which is a linear fDE, and its solution for $p = 1$ is given as (Kilbas and Marzan, 2005),

$$v_1(\eta) = \frac{n_f}{S_0^{1/2}\Gamma(\rho)}\int_0^\eta \frac{\left[\widetilde{R}_e(s) - \tau^{\alpha-1}s^\alpha v_0^{1/m}(\eta)\right]}{(\eta-\xi)^{1-\rho}}d\xi \tag{27}$$

which can be integrated but the integration is in a very complicated form. To offer simpler formulae for practical applications, it can be reasonably assumed that $g_0 = 0$ in the subsequent iterations so that Eq. (27) can be simply integrated term-by-term (Gradshteyn and Ryzhik, 2007, Eq. (3.191)–(1), p. 315) to give,

$$v_1(\eta) = A(t)\eta^\rho + B\eta^{\rho-1+1/m} \tag{28}$$

with

$$A(t) = \frac{(r_0 - A_s)n_f}{\Gamma(\rho+1)S_0^{1/2}} - \frac{\beta S n_f}{(2\lambda-1)\Gamma(\rho+1)S_0^{1/2}}t^{\beta/(2\lambda-1)]-1} \tag{29}$$

and

$$B = \frac{\Gamma(1-\alpha)\Gamma(1/m)n_f\tau^{\alpha-1}}{\alpha\Gamma(\rho+1/m)S_0^{1/2}}t^{-\alpha-1} \tag{30}$$

The two-order HPM approximation to the exact solution of Eq. (18) is given by adding Eqs. (25) and (28) after applying the inverse Laplace transform and restoring the original variables,

$$H(x,t) = \left[H_0^m + \left(H_L^m - H_0^m\right)\frac{x}{L} + A(t)\left(\frac{x}{L}\right)^\rho + B(t)\left(\frac{x}{L}\right)^{\rho-1+1/m}\right]^{1/m} \tag{31}$$

which, for $x = 0$ at the top end of the hillslope, is $H(0,t) = H_0$, as a logical consequence. The solution in Eq. (31) is a two-order approximation only while the exact solution of Eq. (6) is the summation of infinite terms. Eq. (31) implies that the two-order approximate solution of the rfKWE using the HPM accommodates both the linear term, x, and the power functions, x^ρ and $x^{\rho-1+1/m}$. One special case of Eq. (31) is for $m = 2$, which was from field measurements (Horton, 1938; Eagleson, 1970; Emmett, 1970)), then Eq. (31) is simplified as,

$$H(x,t) = \left[H_0^2 + \left(H_L^2 - H_0^2\right)\frac{x}{L} + A(t)\left(\frac{x}{L}\right)^\rho + B(t)\left(\frac{x}{L}\right)^{\rho-1/2}\right]^{1/2} \tag{32}$$

3.2.2. Velocity and unit discharge of overland flow

With the new solution for $H(x,t)$, the conventional velocity in Eq. (4) and the unit discharge in Eqs. (5) have to be updated to account for the nonlocality properties. The change to be introduced is the fractional roughness coefficient, n_f, so that the velocity in Eq. (4) is updated as

$$V = \frac{S_0^{1/2}}{n_f} H^{m-1} \tag{33}$$

which is combined with Eq. (31) to give,

$$V = \frac{S_0^{1/2}}{n_f}\left[H_0^m + \left(H_L^m - H_0^m\right)\frac{x}{L} + A(t)\left(\frac{x}{L}\right)^{\rho} + B(t)\left(\frac{x}{L}\right)^{\rho-1+1/m}\right]^{1-1/m} \tag{34}$$

and the corresponding unit discharge is updated from Eq. (5) and combined with Eq. (31) to yield,

$$q = \frac{S_0^{1/2}}{n_f}\left[H_0^m + \left(H_L^m - H_0^m\right)\frac{x}{L} + A(t)\left(\frac{x}{L}\right)^{\rho} + B(t)\left(\frac{x}{L}\right)^{\rho-1+1/m}\right] \tag{35}$$

With the incorporation of the new roughness coefficient and the changes in the relationships between H and V, and H and q, the flow pattern parameter, m, may deviate from the reported values of $m = 5/3$ for turbulent flow and $m = 3$ for laminar flow.

3.2.3. Solutions of the rfKWE of overland flow with a random rainfall intensity under some special conditions

(1) Steady-state infiltration

After a later time when the terms $t^{[\beta/(2\lambda-1)]-1}$ and $t^{-\alpha-1}$ approach zero, the rate of infiltration approaches to its steady value, then Eq. (29) becomes,

$$A = \frac{(r_0 - A_s)n_f}{\Gamma(\rho+1)S_0^{1/2}} \tag{36}$$

and in Eq. (30) $B(t)\to 0$, then Eqs. (31), (34) and (35) simplify, respectively, as

$$H = \left[H_0^m + \left(H_L^m - H_0^m\right)\frac{x}{L} + \frac{(r_0 - A_s)n_f}{\Gamma(\rho+1)S_0^{1/2}}\left(\frac{x}{L}\right)^{\rho}\right]^{1/m} \tag{37}$$

$$V = \frac{S_0^{1/2}}{n_f}\left[H_0^m + \left(H_L^m - H_0^m\right)\frac{x}{L} + \frac{(r_0 - A_s)n_f}{\Gamma(\rho+1)S_0^{1/2}}\left(\frac{x}{L}\right)^{\rho}\right]^{1-1/m} \tag{38}$$

and

$$q = \frac{S_0^{1/2}}{n_f}\left[H_0^m + \left(H_L^m - H_0^m\right)\frac{x}{L}\right] + \frac{(r_0 - A_s)}{\Gamma(\rho+1)}\left(\frac{x}{L}\right)^{\rho} \tag{39}$$

The last component in Eq. (37) scales with $H \sim x^{\rho/m}$, which is precisely the asymptotic result $H \sim x^{\rho/2}$ presented earlier (Su and Zhang, 2022) for $m = 2$ as a special case. The terms $H_0^m + \left(H_L^m - H_0^m\right)\frac{x}{L}$ in above equations represent the conventional movement while the second terms incorporate the memory-dependent components or nonlocal effects. In the cases $x = 0$ and $r_0 = A_s$, no memory effect is present.

(2) Solutions with steady-state infiltration after the cessation of rainfall

During steady-state infiltration, further simpler cases appear when $r_0 = 0$, and Eqs. (37), (38) and (39) are, respectively, simplified as follows,

$$H = \left[H_0^m + \left(H_L^m - H_0^m\right)\frac{x}{L} - \frac{A_s n_f}{\Gamma(\rho+1)S_0^{1/2}}\left(\frac{x}{L}\right)^{\rho}\right]^{1/m} \tag{40}$$

for the depth of overland flow,

$$V = \frac{S_0^{1/2}}{n_f}\left[H_0^m + \left(H_L^m - H_0^m\right)\frac{x}{L} - \frac{A_s n_f}{\Gamma(\rho+1)S_0^{1/2}}\left(\frac{x}{L}\right)^{\rho}\right]^{1-1/m} \tag{41}$$

for the velocity of overland flow, and

$$q = \frac{S_0^{1/2}}{n_f}\left[H_0^m + \left(H_L^m - H_0^m\right)\frac{x}{L}\right] - \frac{A_s}{\Gamma(\rho+1)}\left(\frac{x}{L}\right)^{\rho} \tag{42}$$

for the unit discharge.

Equations (40), (41) and (42) imply that the effects of nonlocality manifested by the spatial fractional derivatives on the flow are present throughout the flow process until the end of the flow when the values containing the linear part, x and the nonlinear component, x^{ρ}, in these equations are equal.

(3) Situations of overland flow on an impermeable surface after the cessation of rainfall, overland flow with the input and output being equal, and hydrographs at the end of a hillslope

From Eqs. (40), (41) and (42), it is seen that for flow on an impermeable surface which is equivalent to the case $A_s = 0$, or $r_0 = A_s$, the following expressions result for the neglible depth of flow at the upper boundary,

$$H = H_L\left(\frac{x}{L}\right)^{1/m} \tag{43}$$

for the depth of flow,

$$V = \frac{S_0^{1/2}}{n_f}\left(H_L\frac{x}{L}\right)^{m-1} \tag{44}$$

for the velocity, and

$$q = \frac{S_0^{1/2}H_L^m x}{n_f L} \tag{45}$$

for the unit discharge.

Obviously, for $x = L$ at the end of the hillslope, Eq. (44) becomes,

$$V = \frac{S_0^{1/2}}{n_f}H_L^{m-1} \tag{46}$$

which is precisely the original velocity in Eq. (4), and Eq. (45) becomes

$$q = \frac{S_0^{1/2}}{n_f}H_L^m \tag{47}$$

which is precisely the unit discharge in Eq. (5).

These results imply that the widely used methods of the velocity in Eq. (4) and unit discharge in Eq. (5) are only special cases of the solutions of this more generic fractional model, rfKWE, for $r_0 = 0$ and $A_s = 0$ at large time $t\to\infty$ at the end of a hillslope.

(4) Hydrographs at the end of a hillslope

Obviously, for $x = L$ at the end of the hillslope, Eq. (31) becomes,

$$H(x,t) = \left[H_L^m + A(t) + B(t)\right]^{1/m} \tag{48}$$

which is the hydrograph as a function of time and other parameters generated by the rainfall with the intensity of r_0, where $A(t)$ is given by Eq. (29) and $B(t)$ by Eq. (30). For moderate or large times when the microrelief on the slope is filled, $B(t)\to 0$, and Eq. (48) becomes,

$$H(x,t) = \left[H_L^m + A(t)\right]^{1/m} \tag{49}$$

which, after the infiltration reaches its steady state when $t^{[\beta/(2\lambda-1)]-1}\to 0$, becomes,

$$H(x,t) = \left[H_L^m + \frac{(r_0 - A_s)n_f}{\Gamma(\rho+1)S_0^{1/2}}\right]^{1/m} \tag{50}$$

which applies to $x = L$ for large time when infiltration reaches a steady state, and the slope storage no longer affects the flow.

Equation (37) has the following implications in practice, if the roughness and the slope gradients remain unchanged:

(1) after the infiltration reaches a steady state, the depth of overland flow hydrograph at the end of the slope depends only on the depth of flow at the end of the slope, and the rainfall intensity r_0 as a power function, $(r_0 - A_s)^{1/m}$.
(2) after the cessation of a rainfall event, the recession in the depth of flow hydrographs from a hillslope obeys a power function of the form,

$$H(x,t) = \left[H_L^m - \frac{A_s n_f}{\Gamma(\rho+1)S_0^{1/2}}\right]^{1/m} \tag{51}$$

and the corresponding unit discharge is given by the asymptotic form of Eq. (39)

$$q = \frac{S_0^{1/2}}{n_f}\left[H_L^m - \frac{A_s n_f}{\Gamma(\rho+1)S_0^{1/2}}\right] \tag{52}$$

which compares with Eq. (5).

These solutions and their simplifications are partly verifications of the HPM solutions for flow problems on hillslopes. They state that on an infiltrating surface the temporal nonlocality of flow represented by the order of fractional derivatives in time diminishes over time while the spatial nonlocality manifested by the order of fractional derivatives in space continues as long as there is flow on the infiltrating surface. These mechanisms are different from that during infiltration of water into porous soils on a slope where both the temporal and spatial nonlocalities are present throughout the flow processes (see Eq. (10) and Su, 2014, 2020).

3.2.4. The depth of overland flow, velocity and unit discharge for different forms of flow pattens

Depending on the flow patterns, the value of m varies, and it is $m = 5/3$ for turbulent overland flow, $m = 3$ for laminar overland flow, and its value observed in the field is $m \approx 2$ (Horton, 1938; Eagleson, 1970, p. 332). To determine a specific flow quantity using the above equations, different values of m need to be specified. As it can be seen in section 4, the analysis using the rfKWE model with data collected using laboratory flumes yields a consistent result of $m = 1.5$. In the field conditions, its value could be different from $m \approx 2$ for the classic KWE.

3.3. Solutions of the rfKWE with the rainfall intensity and final infiltration rate as a random distribution function

3.3.1. Depth of overland flow

In this section, both the rainfall intensity and the final infiltration rate are treated as random functions. The random gamma probability distribution function (pdf) is chosen for the rainfall intensity (Sen and Eljadid, 1999; Aksoy, 2000),

$$r(t) = \frac{R_0 a^b}{\Gamma(b)} t^{b-1} e^{-at} \tag{53}$$

where R_0 is an amplitude, $\Gamma(b)$ is the gamma function with the argument, b, being a random variable (Braumann et al., 2018) and a is a shape parameter that can be regarded as random but not essential. In addition to the gamma pdf, the exponential pdf can also be used (Eagleson, 1972) to represent a rainfall process.

The equation of infiltration rate in Eq. (10) is still used here except with its final infiltration rate, A_s, being a random variable (Su, 2023). With these generalisations, Eq. (18) is valid here with the random terms in place,

$$\frac{S_0^{1/2}}{n_f}\frac{d^\rho \widetilde{g}(\eta)}{d\eta^\rho} = \widetilde{R}_e(s) - s^\alpha \widetilde{g}^{1/m}(\eta) - \sum_{k=0}^{n-1} s^{\rho-k-1} f^{(k)}(x) \tag{54}$$

and the BCs also take the following forms,

$$\widetilde{g}(\eta) = \widetilde{g}_0, \eta = 0 \tag{55}$$

and

$$\widetilde{g}(\eta) = \widetilde{g}_L, \eta = 1 \tag{56}$$

except for the source term being

$$\widetilde{R}_e(s) = \frac{R_0}{(s+a)^b} - \frac{A_s}{s} - \frac{\beta S}{2\lambda - 1}\frac{\Gamma[\beta/(2\lambda-1)]}{s^{\beta/(2\lambda-1)}} \tag{57}$$

The procedures based on the HPM in section 3.2.1 can be used equally to derive solutions with a different rainfall intensity and infiltration rate. The two-order approximation to the HPM solution of Eq. (54) is

$$v_1(\eta) = C(t)\eta^\rho + D(t)\eta^{\rho-1+1/m} \tag{58}$$

with

$$C(t) = \frac{R_0 a^b n_f}{\Gamma(\rho+1)\Gamma(b)S_0^{1/2}} t^{b-1} e^{-at} - \frac{A_s n_f}{\Gamma(\rho+1)S_0^{1/2}} - \frac{\beta S n_f}{(2\lambda-1)\Gamma(\rho+1)S_0^{1/2}} t^{[\beta/(2\lambda-1)]-1} \tag{59}$$

and

$$D(t) = \frac{\Gamma(1-\alpha)\Gamma(1/m)\tau^{\alpha-1} n_f}{\alpha\Gamma(\rho+1/m)S_0^{1/2}} t^{-\alpha-1} \tag{60}$$

The two-order HPM approximation to the exact solution of Eq. (54), after restoring the original variables, is given as

$$H(x,t) = \left[H_0^m + \left(H_L^m - H_0^m\right)\frac{x}{L} + C(t)\left(\frac{x}{L}\right)^\rho + D(t)\left(\frac{x}{L}\right)^{\rho-1+1/m}\right]^{1/m} \tag{61}$$

3.3.2. Velocity And unit discharge of overland flow

Based on Eq. (61), the velocity in Eq. (4) and the unit discharge in Eqs. (5) can now be updated in a similar way Eqs. (34) and (35) are presented, which are

$$V = \frac{S_0^{1/2}}{n_f}\left[H_0^m + \left(H_L^m - H_0^m\right)\frac{x}{L} + C(t)\left(\frac{x}{L}\right)^\rho + D(t)\left(\frac{x}{L}\right)^{\rho-1+1/m}\right]^{1-1/m} \tag{62}$$

and

$$q = \frac{S_0^{1/2}}{n_f}\left[H_0^m + \left(H_L^m - H_0^m\right)\frac{x}{L} + C(t)\left(\frac{x}{L}\right)^\rho + D(t)\left(\frac{x}{L}\right)^{\rho-1+1/m}\right] \tag{63}$$

3.3.3. Solutions of the rfKWE of overland flow with a random rainfall intensity under some special conditions

(1) Steady-state infiltration

After a certain time when the terms $t^{[\beta/(2\lambda-1)]-1}$ and $t^{-\alpha-1}$ approach zero, the rate of infiltration approaches its steady value, and Eq. (59) becomes,

$$C(t) = \frac{R_0 a^b n_f}{\Gamma(\rho+1)\Gamma(b)S_0^{1/2}} t^{b-1} e^{-at} - \frac{A_s n_f}{\Gamma(\rho+1)S_0^{1/2}} \tag{64}$$

and in Eq. (60) $D(t)\to 0$, then Eqs. (61), (62) and (63) simplify, respectively, as

$$H = \left\{H_0^m + \left(H_L^m - H_0^m\right)\frac{x}{L} + \left[\frac{R_0 a^b n_f t^{b-1} e^{-at}}{\Gamma(\rho+1)\Gamma(b)S_0^{1/2}} - \frac{A_s n_f}{\Gamma(\rho+1)S_0^{1/2}}\right]\left(\frac{x}{L}\right)^\rho\right\}^{1/m} \tag{65}$$

for the depth of flow,

$$V=\frac{S_0^{1/2}}{n_f}\left\{H_0^m+\left(H_L^m-H_0^m\right)\frac{x}{L}+\left[\frac{R_0a^bn_ft^{b-1}e^{-at}}{\Gamma(\rho+1)\Gamma(b)S_0^{1/2}}-\frac{A_sn_f}{\Gamma(\rho+1)S_0^{1/2}}\right]\left(\frac{x}{L}\right)^{\rho}\right\}^{1-1/m} \tag{66}$$

for the velocity, and

$$q=\frac{S_0^{1/2}}{n_f}\left\{H_0^m+\left(H_L^m-H_0^m\right)\frac{x}{L}+\left[\frac{R_0a^bn_ft^{b-1}e^{-at}}{\Gamma(\rho+1)\Gamma(b)S_0^{1/2}}-\frac{A_sn_f}{\Gamma(\rho+1)S_0^{1/2}}\right]\left(\frac{x}{L}\right)^{\rho}\right\} \tag{67}$$

for the unit discharge.

The characteristics of H, V and q in Eqs. (65), (66) and (67) depend on the rainfall patterns which are specified by the parameters R_0, a and b. During a rainfall event when the gamma distribution reaches its recession stage, the term $t^{b-1}e^{-at}$ gradually approaches zero as $t\to\infty$, then the above equations are simplified, respectively, as,

$$H=\left[H_0^m+\left(H_L^m-H_0^m\right)\frac{x}{L}-\frac{A_sn_f}{\Gamma(\rho+1)S_0^{1/2}}\left(\frac{x}{L}\right)^{\rho}\right]^{1/m} \tag{68}$$

$$V=\frac{S_0^{1/2}}{n_f}\left[H_0^m+\left(H_L^m-H_0^m\right)\frac{x}{L}-\frac{A_sn_f}{\Gamma(\rho+1)S_0^{1/2}}\left(\frac{x}{L}\right)^{\rho}\right]^{1-1/m} \tag{69}$$

and

$$q=\frac{S_0^{1/2}}{n_f}\left[H_0^m+\left(H_L^m-H_0^m\right)\frac{x}{L}\right]-\frac{A_s}{\Gamma(\rho+1)}\left(\frac{x}{L}\right)^{\rho} \tag{70}$$

For flow on an impermeable surface with $A_s=0$ after the cessation of rainfall for a considerable time, Eqs. (68), (69) and (70) for the neglible depth of flow at the upper boundary become identical to Eqs. (43), (44) and (45), and the same conclusions apply.

3.4. Explanation of the solutions for the depth of flow, H, velocity, V and unit discharge,q

3.4.1. With a constant or random input,r_0

In Eqs. (31) and (32), the coefficient $A(t)$ given by Eq. (29) consists of two components: the first component is the input to overland flow from the effective rainfall (or the net input), (r_0-A_s) which includes the steady infiltration, and the second component is the absorption by unsaturated surface which recesses over time as $t^{\beta/(2\lambda-1)]-1}$ and eventually approaches zero when the hillslope approaches saturation. The coefficient $B(t)$ characterises the filling of the microrelief on a hillslope during rainfall, and approaches to zero when the microrelief is filled with water. From hydrological practice, it can be found that $t^{\beta/(2\lambda-1)]-1}$ and $t^{-\alpha-1}$ approach to zero after a moderate time.

3.4.2. With a random gamma function input

In section 3.3, a gamma function input is used to derive the expressions for the depth of flow, H, velocity, V, and the unit discharge, q. Similar to the case of a constant or random input, r_0, in *section 3.4.1*, $t^{\beta/(2\lambda-1)]-1}$ and $t^{-\alpha-1}$ in the case of a gamma function input can approach to zero after a moderate time.

While the parameters in the equation of infiltration can be measured and the microrelief filling estimated, the calibration of these full equations require extensive efforts, and further research is needed to address this issue. With this situation in mind, this paper demonstrates the applications of the steady-state solutions only.

4. Determination of model parameters and the interpretation of the results

4.1. Laboratory flume setup and experiments

The data sets used in this study were reported earlier (Zhang et al., 2014, 2015; Zhang and Wang, 2017), where the experimental procedures were described in detail. For the convenience of the readers, the facilities and the experimental procedures used for data collection are briefly outlined below.

The overland flow data were generated by simulated rainfall in a rainfall simulation hall at the State Key Laboratory of Soil Erosion and Dryland Farming on the Loess Plateau, Institute of Soil and Water Conservation, CAS and MWR. One soil type (loessial loamy soil) was used throughout the experiments to be consistent, and the measurements were made on the flume (hillslope) at five lengths (0.4, 0.8, 1.2, 1.6, and 2 m.) with five slope gradients (18 %, 27 %, 36 %, 47 %, and 58 %) and five rainfall intensities (48, 62.4, 102, 149, and 170 $mm.\min^{-1}$). With these scenarios, 125 combinations of data were generated with each having two replicates so that 250 tests were conducted, and the replicate means were determined for further analyses.

The runoff flumes were based on perforated metal sheets with five different lengths, and each flume was 0.4 m wide, and 0.25 m deep. The flumes were adjustable to form different slopes, and the slope gradients from 0 % to 84 % were used to fill the loessial loamy soil. The soil was collected from the 0–25 cm tillage layer on a farmland in the Ansai District, Shaanxi Province, located in the northern Loess Plateau. The air-dried soil with a particle composition of 38.7 % sand, 45.6 % silt, 15.7 % clay, and 0.5 % organic matter was sieved through a 4.0 mm sieve. The sieved soil, with an initial moisture content at approximately 14 %, was packed into the perforated metal plots with four 5.5-cm thick layers totalling a depth of 22 cm with a bulk density of 1.3 $g.cmg.cm^{-3}$. The surface of each layer of the packed soil was lightly roughened each time before the next layer was placed, except for the top surface of the layer left smooth.

A DIK-6000 rainfall simulator by Daiki Riga Kogyo Co., Ltd., Konosu City, Japan was used to generate the simulated rainfall events. This simulator, with the height of 8.67 m and an effective rainfall area of 2 m x 3 m, can produce rain drops with a median diameter of approximately 2.2 mm and a relative uniform rainfall (uniformity >85 %). Each simulated rainfall event lasted for 60 minutes (min.). Prior to the first 15 min of runoff, runoff suspension samples were collected continuously from the plots at intervals of 1 min, 2 min, 3 min, 4 min, and 5 min, respectively, and then at an interval of 5 min. The sheet flow velocity was measured over the lowest 40 cm segment at two positions (10 cm from each side wall) using the dye method with a $KMnO_4$ solution and a stopwatch. The mass of the runoff suspension samples was weighed, and the volume measured immediately after the simulated rainfall. Quantities of sediment and runoff were calculated from the measured volume and weight of the runoff suspension and its density. The mean flow depth for each plot segment was calculated with the mean flow velocities at two positions along with the corresponding total runoff volumes. The velocity of the whole plot was the average of velocities on each segment. Data analysis was performed using the averages of the last six values during the quasi-steady state in each experiment. During the laboratory experiments, majority of the runs produced only inter-rill erosion and very few events produced very small rills at the end of the rainfall.

4.2. Procedures for parameter determination

For simpler models, the model parameters can be directly measured, but for complicated models, any direct measurement will be more difficult, and other procedures such as curve-fitting and interpretation become important. Generally, the difficulty and uncertainty in the parameter determination increase with the increases in the number of model parameters. When the number of parameters in a model is large, a curve fitting process with a computer code could generate fictitious results because an optimal automatic fitting process could only seek an optimal numerical value without prioritising its physical relevance. To find a robust and reliable method for determining the flow parameters in the above solutions with a hydraulically meaningful result, the procedures implemented below include the curve-fitting of the measured unit discharge, q, depth of flow, H, against the distance on the flow path on the hillslope using the code TableCurve2D, then the desired parameters are derived from the optimally fitted parameters.

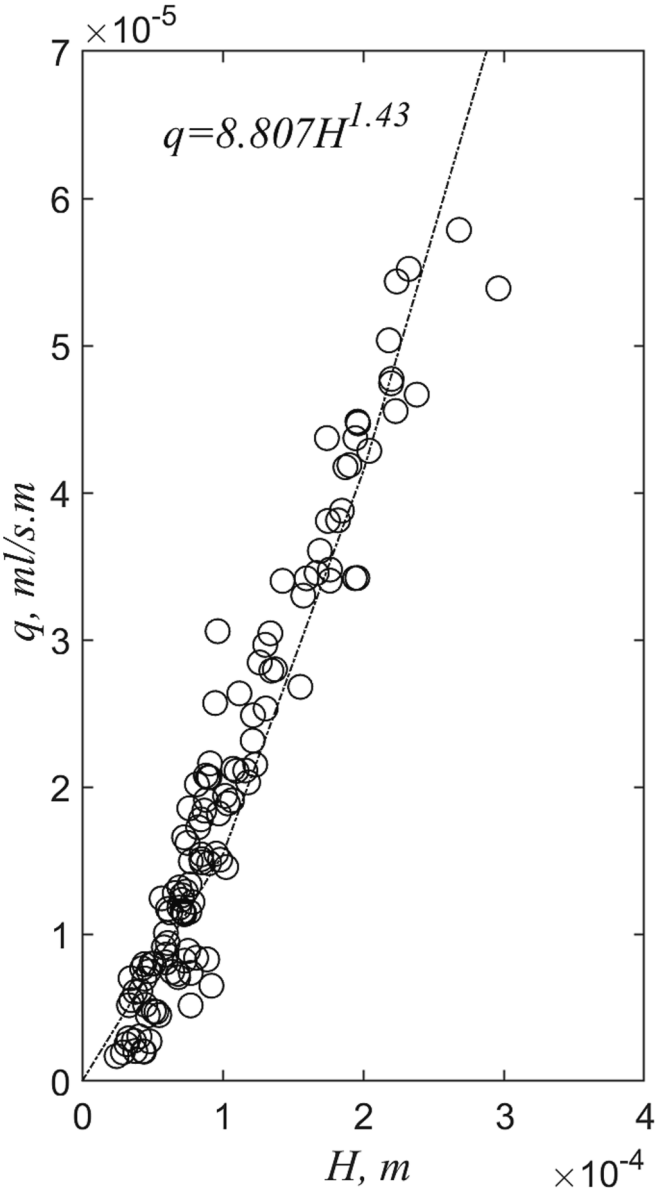

Fig. 1. Determination of the flow pattern parameter m.

4.2.1. Determination Of the flow pattern parameter, m, and the conventional roughness, n, in the KWE

The easiest way for finding the pattern parameter is to fitting Eq. (5) or (4) to the data. With all the collected data are plotted as one sample using Eq. (5), Fig. 1 is generated to show that the value of $m = 1.43$ in the unit discharge-depth relationship for the data used in this paper.

With q, H, and S_0 measured, and m determined from the curve-fitting, the roughness coefficient can be found by rearranging Eq. (5),

$$n = \frac{S_0^{1/2}}{q} H^m \tag{71}$$

By plotting the different data sets for flow depths and unit discharges measured on different slopes, the mean roughness coefficient determined using Eq. (71) is $n = 0.108$, which is also a quantity found for overland flow on a typical *medium, freshly disked fallow* surface (Engman, 1986, Table 4) that is a reasonable description of the repacked soil on the flumes in the laboratory.

Once m against n are estimated, and by plotting all the values of m against n for different experiments under different rainfall intensities and slope gradients, it is found that a clear relationship exists between these parameters as shown in Fig. 2,

The relationship between the two parameters in the conventional kinematic wave equation with the data described in section 4.1 is,

$$m = 1.24 n^{-0.052} \tag{72}$$

which implies that the increase in the roughness on a surface reduces the flow. This is a very straightforward result.

4.2.2. Determination Of the order of the spatial fractional derivatives, ρ, with the data from different locations of a hillslope

The unsteady-state water level in Eq. (31) and subsequent formulae for the velocity in Eq. (34) and the unit discharge in Eq. (35) are characterised with orders of temporal and spatial fractional derivatives for overland flow, α and ρ, and the order of temporal fractional derivatives for infiltration, β. The estimation of these 3 parameters at the same time pose challenges without sufficient information on infiltration, microrelief and overland flow. As a special case of the formulae for the key hydraulic variables, H, V and q, the steady-state formulae in section 3.2.3 are used in this example to demonstrate the application of the new formulae.

Equation (39) for the unit discharge during steady-state infiltration is a better start. For simplicity, the depth of overland flow on the upper boundary, H_0, can be negligibly small in situations during experiments described in this paper so that$H_0 = 0$ is used, then Eq. (39) is rearranged to yield,

$$q = a_0 x + b_0 x^{\rho} \tag{73}$$

where

$$a_0 = \frac{S_0^{1/2} H_L^m}{n_f L} \tag{74}$$

and

$$b_0 = \frac{(r_0 - A_s)}{\Gamma(\rho+1) L^{\rho}} \tag{75}$$

Fitting Eq. (73) to the data collected on different sections of the slope, x, yields the value of ρ, and its mean value from different experiments is $\rho = 1.25$.

4.2.3. Determination Of the fractional roughness coefficient,n_f

First, Eq. (37) is rewritten as, for$H_0 = 0$,

$$H = \left(a_2 x + b_2 x^{\rho}\right)^{1/m} \tag{76}$$

with

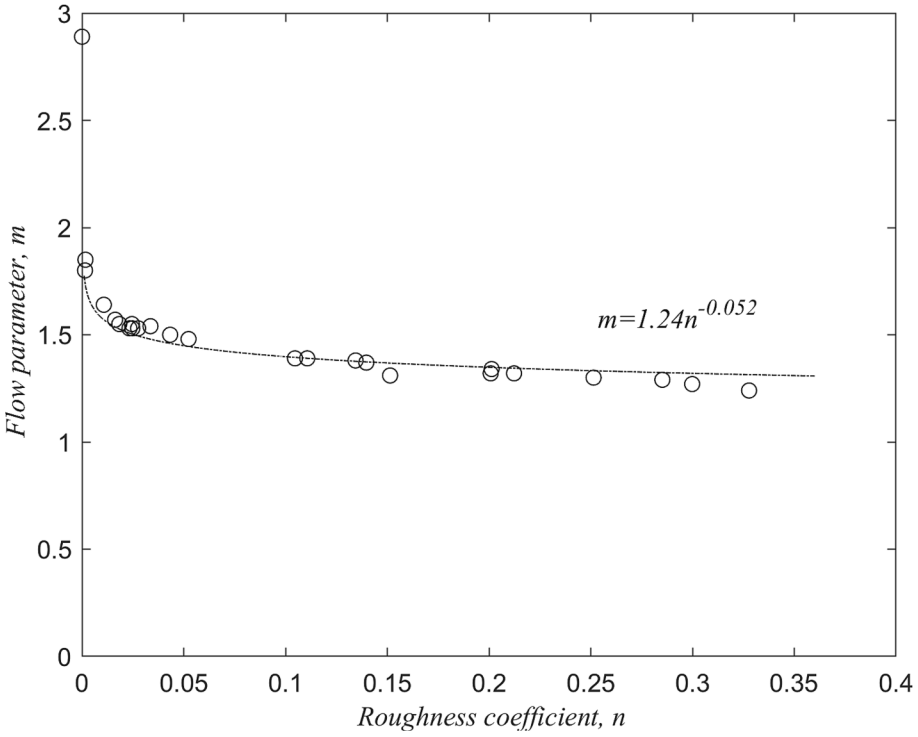

Fig. 2. Relationship between the roughness coefficient and the flow pattern parameter in the classic kinematic wave equation.

$$a_2 = \frac{H_L^m}{L} \tag{77}$$

$$b_2 = \frac{(r_0 - A_s)n_f}{\Gamma(\rho+1)L^\rho S_0^{1/2}} \tag{78}$$

Once b_2 is found by fitting Eq. (76) to the data of H against x, rearranging Eq. (78) to find the fractional roughness coefficient, n_f (see also section 4.2.5 for a more robust form). The analysis has resulted in a mean value of this parameter $n_f = 0.002$.

4.2.4. Determination of the steady-state (or final) infiltration rate on a hillslope, A_s, and ρ.

The initial data analyses with Eq. (73) and the subsequent interpretation of the results indicated that a more robust form to determine the value of ρ is to write Eq. (39) with$H_0 = 0$ in the following form,

$$q = a_0 x + b_1 x^\rho - c_0 x^\rho \tag{79}$$

where

$$b_1 = Dr_0 \tag{80}$$

$$c_0 = DA_s \tag{81}$$

with

$$D = \frac{1}{\Gamma(\rho+1)L^\rho} \tag{82}$$

b_1 and c_0 in Eqs. (80) and (81) are determined through curve-fitting Eq. (79) to the data, which also yields the value of ρ, and the average for the data described in the above experiments is $\rho = 1.25$.

Rearranging Eqs. (80), (81) and (82) yields the steady-state infiltration rate,

$$A_s = \frac{c_0 r_0}{b_1} \tag{83}$$

which is a very useful expression but is impossible to be determined directly when the surface is covered by overland flow.

The further analysis of the flow pattern parameter m and the steady-state infiltration rate is interesting for their representations with A_s for flow into the subsurface while m for flow overland. It is found that these two parameters are closely related as shown in Fig. 3.

Figure 3 implies that the increase in infiltration reduces the quantity

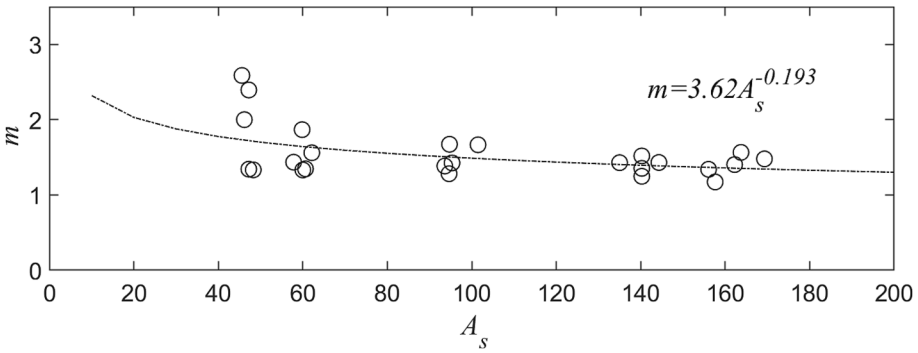

Fig. 3. The relationship between the final infiltration rate and the flow pattern parameter.

of overland flow, which reflects the balance of these two components during the rainfall-runoff processes.

4.2.5. Determination of parameters m and n_f in the rfKWE model

Once the parameter ρ is derived, it is used in Eq. (37) for the depth of overland flow to determine m. First, taking logarithmic transform of Eq. (37) with$H_0 = 0$ yields,

$$\log H = \frac{1}{m}\log(a_2 x + b_2 x^{\rho}) \tag{84}$$

where

$$a_2 = \frac{H_L^m}{L} \tag{85}$$

and

$$b_2 = \frac{(r_0 - A_s)n_f}{\Gamma(\rho+1)S_0^{1/2}L^{\rho}} \tag{86}$$

Similar to Eq. (79), Eq. (84) can be written as follows,

$$\log H = \frac{1}{m}\log(a_2 x + b_3 x^{\rho} + c_1 x^{\rho}) \tag{87}$$

where

$$b_3 = D_2 r_0 \tag{88}$$

and

$$c_1 = -D_2 A_s \tag{89}$$

with

$$D_2 = \frac{n_f}{\Gamma(\rho+1)S_0^{1/2}L^{\rho}} \tag{90}$$

By combining Eqs. (88), (89) and (90), the following expression for the steady-state infiltration rate is found,

$$A_s = -\frac{c_1 r_0}{b_3} \tag{91}$$

Note that the values determined from Eqs. (83) and (91) are identical or at least should be close. It has been found that Eq. (87) is easier and more robust than Eq. (37) to find the value of m during curve fitting processes.

With Eqs. (74) and (77) or Eqs. (74) and (85), an expression for the fractional roughness coefficient, n_f, is found to be

$$n_f = \frac{a_2}{a_0}S_0^{1/2} \tag{92}$$

The values of m and n_f for the data collected in the laboratory described earlier are plotted in Fig. 4,

Figure 4 is the fractional form of Fig. 2 for the two key parameters, and the same explanations apply, i.e., the increase in the fractional roughness coefficient reduces the value of the flow pattern parameter leading to the decrease in the flow velocity and discharges.

4.3. A summary of the derived parameters and their variabilities

With the procedures outlined above, the key model parameters can be derived using data and a curve-fitting code. The analysis of the data from the experiments shows that the flow pattern parameter m decreases slowly as the roughness coefficient increases (Figs. 2 and 4). This trend is logical because the increase in the roughness slows down the flow on the hillslope so that the value of m decreases resulting in the decrease in the velocity and discharge.

There are other inter-relationships between the model parameters, and one of them exits between the order of fractional derivatives and the fractional roughness coefficient in Fig. 5.

Figure 5 clearly indicates that as the roughness of the surface increases the order of fractional derivatives decreases with $\rho = 1$ as the asymptotic value. In other words, the increase in the surface roughness decreases the spatial nonlocality during overland flow processes with the conventional KWE as the asymptotic result. In an earlier study (Su and Zhang, 2022), it was found that the value of ρ varies slowly with the slope gradient and the rainfall intensity.

Another relationship exists between the fractional roughness coefficient and the conventional roughness coefficient as shown in Fig. 6.

The relationship in Fig. 6 can be used to determine the fractional roughness coefficient once a robust relationship is established with sufficient data. This relationship is a useful means for determining the fractional roughness coefficient without other complicated procedures because the conventional roughness coefficient can be easily determined using Eq. (71) or Eq. (5).

With the above procedures the values of the key parameters are determined, and the average values of the parameters that appear in the conventional and fractional models are summarised in Table 1. Note that the definition of the fractional roughness coefficient is different from the original kinematic wave equation so that its value is different.

It should be pointed out here that the length of the 2-metre flumes used in the experiments may not long enough to permit the overland flow to develop full patterns because the flow accelerates as it approaches the end of the flumes due to the decreasing flow resistance, which is like the drawdown effect near a weir. More data on long slopes and natural surfaces are needed to verify how these parameters changes.

4.4. The temporal order of fractional derivatives,α

In section 4.2.2, procedures for determining the spatial order of fractional derivatives and the fractional roughness coefficient are outlined with the data from different locations of a flume representing a hillslope. The simultaneous determination of the temporal order of fractional derivatives, α, and other parameters for infiltration pose

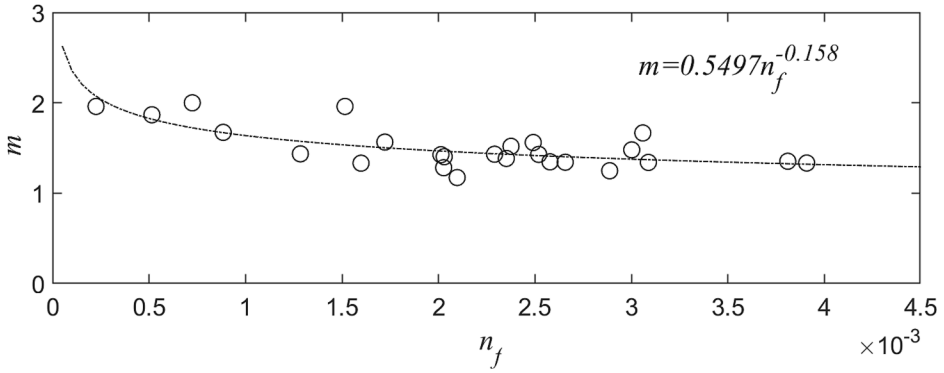

Fig. 4. The relationship between the flow pattern parameter and the fractional roughness coefficient.

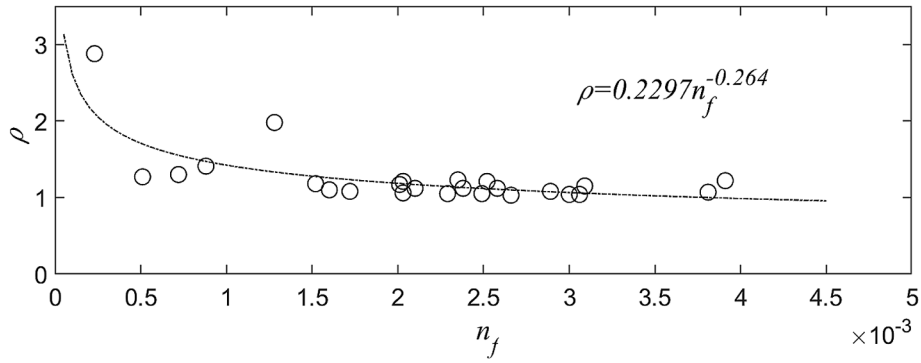

Fig. 5. The inter-relationships between the order of spatial fractional derivatives and the fractional roughness coefficient.

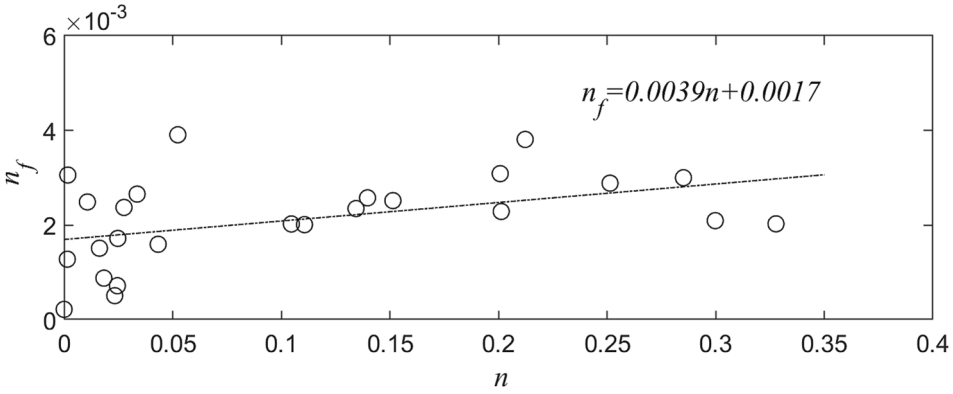

Fig. 6. Relationships between the classic and fractional roughness coefficients.

Table 1
The derived parameters and their variabilities in the two models.

KWE/rfKWE	Classic model		Fractional model			
Parameters	n	m	ρ	n_f	m	A_s, mm/h
Mean	0.108	1.52	1.25	0.0021	1.50	100.94
Standard deviation	0.106	0.327	0.391	0.001	0.232	45.382

challenges without sufficient information on infiltration and filling of microrelief by runoff on a slope. As a special case of the formulae for the key hydraulic variables, H, V and q, the steady-state formulae are demonstrated in this paper only.

5. Comparison of the rfKWE and KWE models for overland flow on a hillslope

As an application of the method presented in this paper and to compare it with the classic KWE, here the overland flow profiles on a hillslope are simulated using Eq. (39) with the parameters summarised in Table 1.

For the new model rfKWE, the mean and standard deviation of each parameter is used to determine the random value of that parameter, e.g., the random value of the fractional roughness coefficient is determined as

$$n_f = \overline{n}_f + 3\sigma f \tag{93}$$

where $\overline{n}_f$ is the mean value of n_f; σ is the standard deviation from the mean $\overline{n}_f$, and f is the random number generator whose values are in $0 < f < 1$. All other parameters such as m, A_s, and r_0 are generated in the same manner. Here 3-fold standard deviation, 3σ, is used, which, of course, can be 1 or 2 times the standard deviation. The mean value for

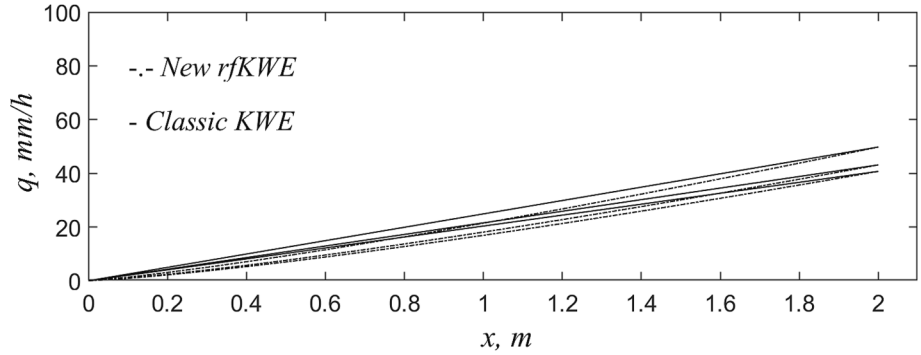

Fig. 7. Applications and comparisons of the classic KWE and the new rfKWE models.

the order of fractional derivatives, ρ, is used only without random fluctuations due to the consideration of uncertain theoretical background to be explored (Casaban *et al.*, 2015).

For the classic KWE, $\rho = 1$ and all other parameters treated as being random determined using Eq. (93), three simulations were run only so that three pairs of profiles were generated as shown in Fig. 7.

It can be seen from Fig. 7 that on the majority of the hillslope, the classic KWE model overestimates the unit discharge compared to that from the rfKWE while the two models yield the same value at the end of the slope, $x/L = 1$. Fig. 7 also demonstrates how the new formulae such as the unit discharge in Eq. (39) is used, which is similar to the velocity in Eq. (38) and the depth in Eq. (37).

6. Conclusions and discussions

This paper presents a time–space random fractional kinematic wave equation (rfKWE) of overland flow with solutions developed using the homotopy perturbation method (HPM) and procedures for estimating the key parameters presented. The key conclusions from the development and applications are as follows:

(1) The rfKWE is featured with two orders of temporal and spatial fractional derivatives with the roughness parameter, the effective rainfall intensity and infiltration rate as random variables or random distributions.
(2) The solutions using the HPM and random Laplace transform incorporate both the initial and boundary conditions are presented for applications. The new solutions are simple with different simplifications presented. The results suggest that on an infiltrating surface the temporal nonlocality of overland flow diminishes over time while the spatial nonlocality exits as long as there is flow on the surface. These results also show that the widely used unit discharge-depth of flow relationship in Eq. (5) is only a special case of a solution of this more generic fractional model.
(3) Procedures for determining the parameters are outlined with examples demonstrating their applications. One important finding is a unique formula for calculating the final infiltration rate or steady-state infiltration rate using data on the depths of overland flow and corresponding unit discharge.
(4) Compared to the fractional kinetic wave equation (fKWE) analysed earlier (Su, 2020; Su and Zhang, 2022), the findings presented in this paper are verified using data from the laboratory, and very useful results come to light, which include the flow pattern parameter, m, the order of spatial fractional derivative, ρ, and fractional roughness coefficient, n_f. With conventional procedures in hydraulics and hydrology, these parameters cannot be easily measured.
(5) The new formulae derived from the rfKWE using the HPM have been demonstrated and compared to the classic KWE model with inputs from the parameters determined using the proposed methods in this paper.
(6) Further work is needed to estimate these parameters for different flow patterns and surface conditions on long slopes and under natural conditions. With data on these forms of hillslopes, it would be clearer to see how the model performs and parameters change. Then predictions of runoff can be made with the new model and robust parameters.

CRediT authorship contribution statement

Ninghu Su: Writing – review & editing, Writing – original draft, Methodology, Formal analysis, Conceptualization. **Fengbao Zhang:** Writing – review & editing, Writing – original draft, Methodology, Formal analysis, Data curation, Conceptualization.

Declaration of competing interest

The authors declare that they have no known competing financial interests or personal relationships that could have appeared to influence the work reported in this paper.

Acknowledgements

The research reported in this paper was partly supported by the National Natural Science Foundation of China (Nos. U22A20613 and 42177338), the “111 Project” (the Overseas Expertise Introduction Center for Discipline Innovation in Soil and Water Conservation and Ecological Restoration) (No. B20052) and the Fundamental Research Funds for the Central Universities (No. 2023HHZX001 and 2452023071). The authors would like to extend their sincere appreciation to the anonymous reviewers whose comments and suggestions helped improve the manuscript of this paper.

Appendix A. Identities in fractional integration and fractional differentiation

In this paper, the Riemann-Liouville (R-L) fractional integration and Caputo fractional differentiation are used in the derivation of the solutions. The readers are referred to Podlubny (1999) for more details on these concepts.

The fractional integration of a function $f(x,t)$ is defined as

$$\mathrm{I}_t^{\beta} f(x,t) = \begin{cases} \dfrac{1}{\Gamma(\beta)} \displaystyle\int_0^t \frac{f(x,\tau)}{(t-\tau)^{1-\beta}} d\tau, & \beta > 0 \\ f(x,t), & \beta = 0 \end{cases} \tag{A1}$$

where $\Gamma(\beta)$ is the gamma function. Eq. (A1) implies that the zero-th order integration of a function $f(x,t)$ is itself, i.e., $\mathrm{I}_t^0 f(x,t) = f(x,t)$.

For the power function, t^{γ}, the following identity holds,

$$\mathrm{I}_t^{\beta} t^{\gamma} = \frac{\Gamma(1+\gamma)}{\Gamma(1+\gamma+\beta)} t^{\gamma+\beta} \tag{A2}$$

Caputo fractional differentiation of a function $f(x,t)$ is given as

$$D_t^{\beta} f(x,t) = \frac{1}{\Gamma(1-\beta)} \int_0^t \frac{1}{(t-\tau)^{\beta}} \frac{\partial f(x,\tau)}{\partial \tau} d\tau, \qquad 0 < \beta < 1 \tag{A3}$$

and the zero-th order fractional differentiation of the function $f(x,t)$ is the function itself, i.e., $D_t^0 f(x,t) = f(x,t)$.

The Caputo fraction differentiation of a power function is given as

$$D_t^{\beta} t^{\gamma} = \frac{\Gamma(1+\gamma)}{\Gamma(1+\gamma-\beta)} t^{\gamma-\beta} \tag{A4}$$

The other useful identities include the following:

$$I_t^{\beta} D_t^{\beta} f(x,t) = f(x,t) - f(x,0) \tag{A5}$$

where $f(x,0)$ is the initial value of $f(x,t)$, and

$$D_t^{\beta} I_t^{\beta} f(x,t) = f(x,t) \tag{A6}$$

Appendix B. Essentials for the homotopy perturbation method (HPM)

The HPM was proposed by He in 1999 as a modified method developed by Liao (1992, 1995, 1997), and its applications have been extraordinarily successful. This method has been applied to solve many types of ODEs, PDEs and their fractional counterparts. In water engineering and hydrology, Kumbahakar and Singh (2023) have summarised a number of examples. For more details on this topic, the reader is referred to other related materials (He, 1999, 2003; Kumbahakar and Singh, 2023). Here only the essentials of this method are outlined, and the procedures most relevant to the fKWE in this paper are detailed in this appendix.

Central to the homotopy perturbation methods and related methods such as homotopy analysis method (HAM) is the concept of homotopy in topology. Topology is a field in mathematics concerned with geometric properties of a mathematical object that remains unaffected under continuous deformation (Kumbahakar and Singh, 2023). Homotopy defines a connection between two mathematical objects, and the two objects are homotopic if one can be continuously deformed into the other, which is the key for approximate solutions in a series when the original problem is expanded in a mathematical expression known as the homotopy.

For example, for two functions, $f(t)$ and $g(t)$, of a dimension t (either for time or space), a homotopy is defined as

$$H(t;q) = (1-q)f(t) + qg(t) \tag{B1}$$

which is defined in the range of zero and one, i.e., $q \in [0,1]$, where q is called the perturbation parameter or embedding parameter. The homotopy $H(t;q)$ between these two functions, $f(t)$ and $g(t)$, is itself a continuous function, and Eq. (B1) clearly shows that $H(t;q) = f(t)$ for $q = 0$ and $H(t;q) = g(t)$ for $q = 1$.

For ODEs, PDEs and their fractional counterparts, the HPM has been applied to derive solutions in a series form (He, 1999). For a general differential operator which can be an operator for ordinary, partial or fractional differentiation, D, and an analytical function, $f(r)$,

$$D(u) = f(r) \tag{B2}$$

where D can be split into two parts, N for a nonlinear operator and L for a linear operator. Then a nonlinear differential equation can be written as

$$N(u) + L(u) - f(r) = 0 \tag{B3}$$

A homotopic of the general differential equation in (B2) (He, 1999; Ates and Zegling, 2017) is

$$H(v,p) = (1-p)[L(v) - L(u_0)] + p[D(v) - f(r)] = 0, \quad p \in [0,1] \tag{B4}$$

where u_0 is the initial approximation of Eq. (B2), and note that the series decomposition solution is defined in terms of v as an approximation to u. Eq. (B4) can also be written as

$$H(v,p) = L(v) - L(u_0) + pL(u_0) + p[N(v) - f(r)] = 0, \quad p \in [0,1] \tag{B5}$$

Eqs (B4) and B5) mean that

$$H(v,0) = L(v) - L(u_0) = 0 \tag{B6}$$

and

$$H(v,1) = D(v) - f(r) = 0 \tag{B7}$$

With p being the perturbation parameter, the solution of Eqs. (B4) or (B5) is assumed to take a series form of,

$$\begin{aligned} v(x,p) &= v_0(x) + v_1(x)p + v_2(x)p^2 + \ldots + \\ &= \sum_{k=0}^{\infty} v_k(x)p^k \end{aligned} \tag{B8}$$

which, for $p = 1$, gives the desired solution of Eq. (B4) or (B5) as

$$\begin{aligned} v(x,p) &= v_0(x) + v_1(x) + v_2(x) + \ldots + \\ &= \sum_{k=0}^{\infty} v_k(x) \end{aligned} \tag{B9}$$

The accuracy of the HPM in solving nonlinear and complex fluid flow problems has been very satisfactory following comparisons with the traditional approximation methods (He, 2003) and classic numerical methods such as the Runge-Kutta (Hatami et al., 2016). This innovative method has been applied to solve various types of nonlinear problems as an alternative to traditional numerical methods (Mohyud-Din et al., 2009).

Data availability

Data will be made available on request.

References

Adomian, G., 1970. Random operator equations in mathematical physics I. J. Math. Phys. 11 (3), 1069–1084.

Adomian, G., 1976. Nonlinear stochastic differential equations. J. Math. Anal. & Appl. 55, 441–452.

Adomian, G., 1990. A review of the decomposition method and some recent results for nonlinear equations. Math. Comput. Modelling. 13 (7), 17–43.

Aksoy, H., 2000. Use of gamma distribution in hydrological analysis. Turk. J. Eng. Environ. Sci. 24, 419–428.

Allmaras, R.R., Burwell, R.E., Larson, W.E., Holt, R.F., 1966. Total porosity and random roughness of the interrow zone as influenced by tillage. USDA. Conserv. Res. Rep. 7, 22 pp.

Ates, I., Zegling, P.A., 2017. A homotopy perturbation method for fractional-order advection-diffusion-reaction boundary-value problems. Appl. Math. Model. 47, 425–441.

Benchohra, M., Hamani, S., Ntouyas, S.k., 2009. Boundary value problems for differential equations with fractional order and nonlocal conditions. Nonlinear Aanl. 71, 2391–2396.

Benson, D.A., Meerschaert, M.M., Revielle, J., 2013. Fractional calculus in hydrologic modeling: A numerical perspective. Adv. Water Resour. 51, 479–497.

Braumann, C.A., Cortés, J.-C., Jódar, L., Villafuerte, L., 2018. On the random gamma function: Theory and computing. J. Comput. Appl. Math. 335, 142–155.

Burgos, C., Cortés, J.-C., Villafuerte, L., Villanueva, R.J., 2022. Solving random fractional second-order linear equations via the mean square Laplace transform: Theory and statistical computing. Appl. Math. Comput. 418 (126846), 1–17.

Burwell, R.E., Allmaras, R.R., Amemiya, M., 1963. A field measurement of total porosity and surface microrelief of soils. Soil Sci. Soc. Am. Proc. 27, 697–700.

Casabán, M.-C., Cortés, J.-C., Jódar, L., 2015. A random Laplace transform method for solving random mixed parabolic differential equations. Appl. Math. Comput. 259, 654–667.

Chow, V.T., Maidment, D.R., Mays, L.W., 1988. Applied Hydrology. McGraw-Hill, New York, USA.

Chowdhury, M.S.H., Hashim, I., Abdulaziz, O., 2009. Comparison of homotopy analysis method and homotopy-perturbation method for purely nonlinear fin-type problems. Communication in Nonlinear Science & Numerical Simulation. 14, 371–378.

Eagleson, P.S., 1970. Dynamic Hydrology. McGraw-Hill, New York, USA.

Eagleson, P.S., 1972. Dynamics of flood frequency. Water Resour. Res. 8 (4), 878–898.

Emmett, W.W., 1970. The hydraulics of overland flow on hillslopes. Geol. Survey Prof. Paper 662-A, USGS, Washington, D.C.

Engman, E., 1986. Roughness coefficient for routing surface runoff. J. Irri. Drain. Eng. 112 (1), 39–53.

Gradshteyn, I.S., Ryzhik, I.M., 2007. Table of Integrals, Series, and Products, 7th ed. Academic Press, Amsterdam.

Harman, C.J., Reeves, D.M., Baeumer, B., Sivapalan, M., 2010. A subordinated kinematic wave equation for heavy-tailed flow responses from heterogeneous hillslopes. J. Geophys. Res. 115, F00A08.

Hatami, M., Hatami, J., Jafaryar, M., Domairry, G., 2016. Differential transformation method for Newtonian and Non-Newtonian fluids flow analysis: comparison with HPM and numerical solution. J. Braz. Soc. Mech. Sci. Eng. 38, 589–599.

He, J.H., 1999. Homotopy perturbation technique. Comput. Methods Appl. Mech. Eng. 178, 257–262.

He, J.H., 2003. Homotopy perturbation method: a new nonlinear analytical technique. Applied Math. Comput. 135, 73–79.

Hopmans, J.W., 1989. Stochastic description of field-measured infiltration data. Trans. ASAE. 32 (6), 1987–1993.

Horton, R.E., 1938. The investigation and application of runoff plot experiments with reference to soil erosion problems. *Proc. Soil Sci. Soc. Am*Er. 3, 340–349.

Javidi, M., Ahmad, B., 2013. Numerical solution of fractional partial differential equations by numerical Laplace inversion technique. Adv. Diff. Eqs. 2013 (375), 1–18.

Javidi, M., Raji, A., 2011. Combination of Laplace transform and homotopy perturbation method to solve the parabolic partial differential equations. Commun. Frac. Calc. 3 (1), 10–19.

Kavvas, M.L., Ercan, A., 2015. Fractional governing equations of diffusion wave and kinematic wave open-channel flow in fractional time-space. I. Development of the equations. J. Hydrol. Eng. 20 (9), 04014096.

Kavvas, M.L., Ercan, A., 2017. Time-space fractional governing equations of unsteady open channel flow. J. Hydrol. Eng. 22 (2), 04016052.

Kavvas, M.L., Ercan, A., Tu, 2021. Space and time fractional governing equations of unsteady overland flow. J. Hydrol. Eng. 26 (7), 04021023.

Kilbas, A.A., Marzan, S.A., 2005. Nonlinear differential equations with the Caputo fractional derivative in the space of continuously differentiable functions. Diff. Eqs. 41 (1), 84–89.

Kuipers, H., 1957. A relief meter for soil cultivation studies. Neth. J. Agric. Sci. 5, 255–262.

Liao, S.J., 1992. A second-order approximate analytical solution of a simple pendulum by the process analysis method. J. Appl. Mech. 59 (4), 970–975.

Liao, S.J., 1995. An approximate solution technique not depending on small parameters: a special example. Int. J. Non-Linear Mech. 30 (3), 371–380.

Liao, S., 1997. Boundary element method for general nonlinear differential operators. Eng. Anal. Boundary Elements. 20 (2), 91–99.

Lighthill, M.H., Whitham, G.B., 1955. On kinematic waves. I. Flood movement in long rivers. Proc. Royal Soc. Ser. a. 229, 281–316.

Mohyud-Din, S.T., Noor, M.A., Noor, K.I., 2009. Some relatively new techniques for nonlinear problems. Math. Prob. Eng. 234849, 1–25.

Philip, J.R., 1991. Hillslope infiltration: Planar slopes. Water Resour. Res. 27 (1), 109–117.

Podlubny, I., 1999. Fractional Differential Equations. Acad. Press, San Diego, California.

Rajabi, A., Ganji, D.D., Taherian, H., 2007. Application of homotopy perturbation method in nonlinear heat conduction and convection equations. Phys. Lett. a. 360, 570–573.

Sajid, M., Hayat, T., 2008. Comparison of HAM and HPM methods in nonlinear heat conduction and convection equations. Nonlinear Anal.: Real World Appl. 9, 2296–2301.

Sen, Z., Eljadid, A.G., 1999. Rainfall distribution function for Libya and rainfall prediction. Hydrol. Sci. J. 44 (5), 665–680.

Su, N., 2010. Theory of infiltration: Infiltration into swelling soils in a material coordinate. J. Hydrol. 395, 103–108.

Su, N., 2014. Mass-time and space-time fractional partial differential equations of water movement in soils: Theoretical framework and application to infiltration. J. Hydrol. 519, 1792–1803.

Su, N., 2017. The fractional boussinesq equation of groundwater flow an its applications. J. Hydrol. 547, 403–412.

Su, N., 2020. Fractional Calculus for Hydrology, Soil Science and Geomechanics. CRC Press, Boca Raton https://www.taylorfrancis.com/books/mono/10.1201/9781351032421/fractional-calculus-hydrology-soil-science-geomechanics-ninghu-su.

Su, N., 2023. Random fractional partial differential equations and solutions for water movement in soils: Theory and applications. Hydrol. Proc. 37, e14844.

Su, N., Zhang, F., 2022. Anomalous overland flow on hillslopes: A fractional kinematic wave model, its solutions and verification with data from laboratory observations. J. Hydrol. 604, 127202.

Villafuerte, L., Braumann, C.A., Cortés, J.-C., Jódar, L., 2010. Random differential operational calculus: Theory and applications. Compu. Math Appl. 59, 115–125.

Yildirim, A., Kocak, H., 2009. Homotopy perturbation method for solving the space-time fractional advection-dispersion equation. Adv. Water Resour. 32, 1711–1716.

Zhang, Y., Benson, D.A., Reeves, D.M., 2009. Time and space nonlocalities underlying fractional-derivative models: Distinction and literature review of field applications. Adv. Water Resour. 32, 561–581.

Zhang, Y., Chen, L., Reeves, D., Sun, H., 2016. A fractional-order tempered-stable continuity model to capture surface water runoff. J. Vibration & Control. 22 (8), 1993–2003.

Zhang, Y., Baeumer, B., Chen, L., Reeves, D., Sun, H., 2017. A fully subordinated linear flow model for hillslope subsurface stormflow. Water Resour. Res. 53, 3491–3504.

Zhang, F., Wang, Z., Yang, M., 2014. Validating and improving interrill erosion equations. PLoS One 9 (2), e88275.

Zhang, F.B., Wang, Z.L., Yang, M.Y., 2015. Assessing the applicability of the Taguchi design method to an interrill erosion study. J. Hydrol. 521, 65–73.

Zhang, X.C., Wang, Z.L., 2017. Interrill soil erosion processes on steep slopes. J. Hydrol. 548, 652–664.

Zobeck, T.E., Onstad, C.A., 1987. Tillage and rainfall effects on random roughness: A review. Soil & Tillage Res. 9 (1), 1–20.